



Research Paper

# Upconversion Nanophosphors $\text{NaLuF}_4:\text{Yb,Tm}$ for Lymphatic Imaging *In Vivo* by Real-Time Upconversion Luminescence Imaging under Ambient Light and High-Resolution X-ray CT

Yun Sun, Juanjuan Peng, Wei Feng and Fuyou Li 

Department of Chemistry, Fudan University, 220 Handan Road, Shanghai 200433, P.R. China

 Corresponding author: Fuyou Li, Email: fyli@fudan.edu.cn

© Ivyspring International Publisher. This is an open-access article distributed under the terms of the Creative Commons License (<http://creativecommons.org/licenses/by-nc-nd/3.0/>). Reproduction is permitted for personal, noncommercial use, provided that the article is in whole, unmodified, and properly cited.

Received: 2012.08.31; Accepted: 2012.10.09; Published: 2013.04.23

## Abstract

Lanthanide upconversion nanophosphor (UCNP) has attracted increasing attention for potential applications in bioimaging due to its excellence in deep and high contrast imaging. To date, most upconversion imaging applications were demonstrated in dark surroundings without ambient light for higher signal-to-noise ratio, which hindered the application of optical imaging guided surgery. Herein, the new established  $\text{NaLuF}_4$ -based UCNP ( $\text{NaLuF}_4:\text{Yb,Tm}$ , ~17 nm) with bright upconversion emission around 800 nm as imaging signal was used to realize imaging under ambient light to provide more convenient for clinician. Moreover, due to the existence of heavy element lutetium (Lu) in the host lattice, the  $\text{NaLuF}_4:\text{Yb,Tm}$  nanoparticles can also be used as an X-ray CT imaging agent to enhance the imaging depth and *in vivo* imaging resolution.

Key words: Lanthanide, upconversion luminescence, lutetium, computed tomography, bioimaging

## Introduction

Multimodal imaging has attracted increasing attentions, because different molecular imaging methods provide different spatial resolution, imaging depth, and areas of application.[1] For example, X-ray computed tomography (CT) imaging gives more atomic detail in living animals than other *in vivo* imaging tools, based on differential X-ray absorption, to show the tissues such as bone and calcifications composed of elements with high atomic number within the body.[2-4] Fluorescence imaging provides a sole tool for visualizing living biosamples from cell to animal.[5] Nevertheless, photoluminescence imaging can only achieve millimeter resolution in the *in vivo* observation, which is poorer than those of CT (~50  $\mu\text{m}$ ), and also limited by poor imaging depth.[6] By combining fluorescence imaging and CT imaging,

the ability to accurately track biological behavior in specified sites *in vivo* could be achieved. Therefore, it is required to develop multifunctional materials for multi-modality molecular imaging.

Due to their unique 4f electron structure, lanthanide ions provide rich optical, electronic, and magnetic properties.[7-11] And thus the lanthanide-based nanoparticles have been explored as imaging agents for luminescence imaging, magnetic resonance imaging (MRI), X-ray CT, and positron emission tomography (PET) and single photon emission computed tomography (SPECT).[4, 11-16] In particular, lanthanide-based nanoparticles for upconversion luminescence (UCL) imaging *in vivo* of whole-body animals have attracted increasing attentions. When the host is co-doped with  $\text{Yb}^{3+}$  as a sensi-

tizer, and  $\text{Er}^{3+}$  or  $\text{Tm}^{3+}$  as an emitter, lanthanide-based nanoparticles show unique UCL emission under continuous-wave excitation at 980 nm,[17-44] with sharp emission lines, large anti-Stokes shift of several hundred nanometers, non-photoblinking, and superior photostability. Using such lanthanide-based upconversion nanophosphors (UCNPs) as photoluminescent probes, the high-contrast bioimaging of living cells and whole-body small animals has been achieved, with low autofluorescence and excellent penetration depth.[8, 26] However, previously reported UCL imaging was performed in dark box to increase the signal-to-noise ratio (SNR), which hindered the operation of researcher and clinician.

On the other hand, realtime and facile lymphatic imaging is considered as an urgent problem faced in clinical because lymphatic metastasis is one of the two main metastasis pathway, and the lymphatic drainage has high individual variability. In the surgical operation, the lymph node and lymphatic vessel must be cleared completely to decrease the neoplasm recurrence.[45, 46] Thus, lymphatic imaging is important for tumor metastasis diagnosis and its surgical operation. In previous studies, lymphatic imaging by fluorescence imaging is limited because of the presence of autofluorescence from biological sample and low SNR.[46] Even using UCL imaging, the lymph node imaging other than lymph vessel imaging has been achieved to date.

In this present study, we developed  $\text{NaLuF}_4$ -based upconversion nanoparticles for dual-modal imaging of lymphatic vessel through combining upconversion luminescence imaging and X-ray CT imaging. Our design strategy of choosing  $\text{NaLuF}_4$  as host is based on the fact that the lutetium ( $\text{Lu}^{3+}$ ) ion has full-occupied f-electron, large atomic number of 71, and high electron density of  $9.85 \text{ g/cm}^3$ . The X-ray attenuation coefficient depends on the atomic number and electron density of the CT agent; the higher the atomic number and electron density, the higher the attenuation coefficient.[47] Therefore, theoretically,  $\text{NaLuF}_4$  nanocrystals could provide effective simultaneous X-ray absorption. At the same time,  $\text{NaLuF}_4$  as host has been reported to show excellent upconversion luminescence property. We also developed the method for upconversion luminescence imaging *in vivo* under ambient light.

## Materials and methods

All the starting materials were obtained from commercial supplies and used as received. Rare-earth oxides  $\text{Lu}_2\text{O}_3$  (99.999%),  $\text{Yb}_2\text{O}_3$  (99.999%), and  $\text{Tm}_2\text{O}_3$  (99.999%) were purchased from Shanghai Yuelong New Materials Co. Ltd. Oleic acid (>90%) was pur-

chased from Alfa Aesar Co., Ltd. 1-octadecene (ODE) (>90%) was purchased from Aladdin Reagent Co., Ltd.  $\text{NaOH}$ ,  $\text{NH}_4\text{F}$ , methanol, ethanol, cyclohexane, hydrochloric solution were purchased from Sinochem Chemical Reagent Co., China. Rare-earth chlorides ( $\text{LnCl}_3$ , Ln: Lu, Yb and Tm) were prepared by dissolving the corresponding metal oxide in 10% hydrochloric solution at elevated temperature and then evaporating the water completely. All other chemical reagents were of analytical grade and were used directly without further purification. Deionized water was used throughout the experiments.

## Characterization

Powder X-ray diffraction (XRD) measurements were performed on a Bruker D4 diffractometer at a scanning rate of  $1^\circ/\text{min}$  in the  $2\theta$  range from  $10$  to  $70^\circ$  ( $\text{Cu K}\alpha$  radiation,  $\lambda = 1.54056 \text{ \AA}$ ). The size and morphology of the nanoparticles were determined at a JEOL JEM-2010 low to high resolution transmission electron microscope (HR-TEM) operated at 200 kV. These as-prepared samples were dispersed in cyclohexane and dropped on the surface of a copper grid for TEM test. Dynamic light scattering (DLS) experiment was carried out on an ALV-5000 spectrometer-goniometer equipped with an ALV/LSE-5004 light scattering electronic and multiple tau digital correlator and a JDS Uniphase He-Ne laser (632.8 nm) with an output power of 22 mW. The size distribution was measured at  $25^\circ\text{C}$  with a detection angle of  $90^\circ$ . The upconversion luminescence (UCL) emission spectrum was recorded on Edinburgh LFS-920 instrument, but the excitation source using an external 0-1 W adjustable 980 nm semiconductor laser (Beijing Hi-Tech Optoelectronic Co., China) with an optic fiber accessory, instead of the Xeon source in the spectrophotometer. All the photoluminescence studies were carried out at room temperature. The photo of upconversion luminescence emission was obtained digitally on a Nikon multiple CCD Camera.

## Synthesis of oleic acid (OA) capped $\text{NaLuF}_4\text{:Yb,Tm}$ nanocrystals

$\text{NaLuF}_4\text{:Yb,Tm}$  nanocrystals have been synthesized according to the previously reported method with some modification.[23] In a typical experiment, 1 mmol  $\text{LnCl}_3$  (RE=Lu, Yb, Tm) with rare earth ions molar ratio of 79:20:1 were added to a 100 mL flask containing 6 mL oleic acid and 15 mL 1-octadecene (ODE). The mixture was heated to  $140^\circ\text{C}$  for 40 min to obtain a clear solution and then cooled down to  $80^\circ\text{C}$ . Solid  $\text{NH}_4\text{F}$  (4 mmol) and  $\text{NaOH}$  (2.5 mmol) were then added into the bottle and degassed at  $120^\circ\text{C}$  for 30 min. The mixture was heated to  $300^\circ\text{C}$  with a heating rate of about  $40^\circ\text{C}/\text{min}$  and maintained at

300 °C in argon atmosphere for 1 h. After cooled down to room temperature, the sample was precipitated by adding mixed liquor of 20 mL ethanol and 10 mL cyclohexane and collected by centrifugation at 14000 rpm. After washing with ethanol and cyclohexane for several times, NaLuF<sub>4</sub>:Yb,Tm nanocrystals were finally redispersed in cyclohexane.

### Synthesis of water-soluble NaLuF<sub>4</sub>:Yb,Tm nanocrystals modified by citrate acid (cit-NaLuF<sub>4</sub>:Yb,Tm)

The preparation of water-soluble cit-NaLuF<sub>4</sub>:Yb,Tm nanocrystals was performed through ligand free nanocrystals as intermediate.[48] 10 mg OA-NaLuF<sub>4</sub>:Yb,Tm was washed with hydrochloric acid (pH = 4) to obtain water-dispersible, ligand-free NaLuF<sub>4</sub>:Yb,Tm nanocrystals. Then ligand-free NaLuF<sub>4</sub>:Yb,Tm was dispersed in the aqueous solution of citrate acid (30 mg/mL) and the cit-NaLuF<sub>4</sub>:Yb,Tm was obtained. The cit-NaLuF<sub>4</sub>:Yb,Tm was washed with water three times for further use.

### UCL imaging of the lymphatic vessel

For *in vivo* UCL imaging under ambient light, a new *in vivo* UCL imaging system was set. The system includes an andor's iXon plus EMCCD camera (DU897), ring shaped 980 nm laser source, fluorescent lamp and mechanical support. EMCCD camera fitted with a band pass filter at 800 nm to block excitation laser. Ring shaped 980 nm laser source was constituted with eight external 0-5 W adjustable CW 980 nm lasers and the laser light has been calibrated to be uniform at the objective table.

For UCL imaging of the lymphatic vessel, 0.05 mL cit-NaLuF<sub>4</sub>:Yb,Tm nanocrystals were subcutaneously injected into the paw footpad of nude mouse. Then the mouse was imaged under ambient light (fluorescent lamp, 50 W) by the *in vivo* UCL imaging system with a ring shaped 980 nm laser (50 mW/cm<sup>2</sup>).

### CT imaging of lymphatic vessel

The mouse treated in the UCL imaging was transferred to a micro-CT scanner (Skyscan 1076: Skyscan, Antwerp, Belgium). A scan lasted about 20 min, resulting in shadow projections with a pixel size of 10 μm. A modified Feldkamp algorithm, using undersampling to reduce noise, was applied to the scan data, resulting in reconstructed 3D data sets with a voxel size of 20 μm.

### In vitro cytotoxicity assay

*In vitro* cytotoxicity was measured by performing methyl thiazolyl tetrazolium (MTT) assay

on the KB cells. Cells were seeded into a 96-well cell culture plate at 5×10<sup>4</sup>/well, under 100% humidity, and were cultured at 37 °C and 5% CO<sub>2</sub> for 12 h. After removal of the culture medium, 100 μL of different concentrations of cit-NaLuF<sub>4</sub>:Yb,Tm (0, 200, 400, 600, 800 and 1000 mg/mL, diluted in RPMI 1640 with 10% FBS) were added to the wells. The cells were subsequently incubated for 48 h at 37 °C under 5% CO<sub>2</sub>. Thereafter, MTT (10 μL; 5 mg/mL) was added to each well and the plate was incubated for an additional 4 h at 37 °C under 5% CO<sub>2</sub>. 10 min after the addition of 100 μL of DMSO to each well, the optical density OD<sub>570</sub> value (Abs.) of each well, with background subtraction at 690 nm, was measured by means of a Tecan Infinite M200 monochromator-based multifunction microplate reader. The following formula was used to calculate the inhibition of cell growth: Cell viability(%)=(mean of Abs. value of treatment group/mean Abs. value of control)×100%.

## Results and Discussion

NaLuF<sub>4</sub> nanocrystals co-doped with 79 mol% Lu<sup>3+</sup>, 20 mol% Yb<sup>3+</sup>, and 1 mol% Tm<sup>3+</sup> were synthesized via a modified solvothermal method.[23] The as-prepared oleic acid coating nanoparticles are denoted as OA-NaLuF<sub>4</sub>:Yb,Tm here. As determined by transmission electron microscopy (TEM), the OA-NaLuF<sub>4</sub>:Yb,Tm have spheric shape with an average size of ~17 nm, as shown in Fig. 1a and b. The peaks in X-ray diffraction (XRD) patterns can be well indexed to the hexagonal phase NaLuF<sub>4</sub> (JCPDS No. 27-0726, Fig. 1c). Energy dispersive X-ray analysis (EDXA) indicates the presence of Lu, Yb, and F elements in the OA-NaLuF<sub>4</sub>:Yb,Tm (Fig. 1d).

Under excitation from a CW 980 nm laser, the OA-NaLuF<sub>4</sub>:Yb,Tm in cyclohexane showed two characteristic upconversion luminescence (UCL) emission bands centered at 475 and 800 nm (Fig. 2), originated from the <sup>1</sup>G<sub>4</sub>→<sup>3</sup>H<sub>6</sub> and <sup>3</sup>H<sub>4</sub>→<sup>3</sup>H<sub>6</sub> transitions of Tm<sup>3+</sup>, respectively. In particular, OA-NaLuF<sub>4</sub>:Yb,Tm exhibited an excellent 800 nm near infrared (NIR) UCL emission. The inset of Fig. 2 is the photograph of the sample, and a blue UCL emission is visible to the naked eye directly.

To achieve better dispersion of the nanoparticles in water, citric acid (cit) was used as surface ligand to replace the oleic acid of the OA-NaLuF<sub>4</sub>:Yb,Tm.[49] The obtained citric acid-modified nanoparticles are described here as cit-NaLuF<sub>4</sub>:Yb,Tm. The cit-NaLuF<sub>4</sub>:Yb,Tm showed excellent water-solubility, and had a hydrodynamic size of ~25 nm (Supplementary Material: Fig. S1), with a zeta potential of ~-33.3 mV (Supplementary Material: Fig. S2).

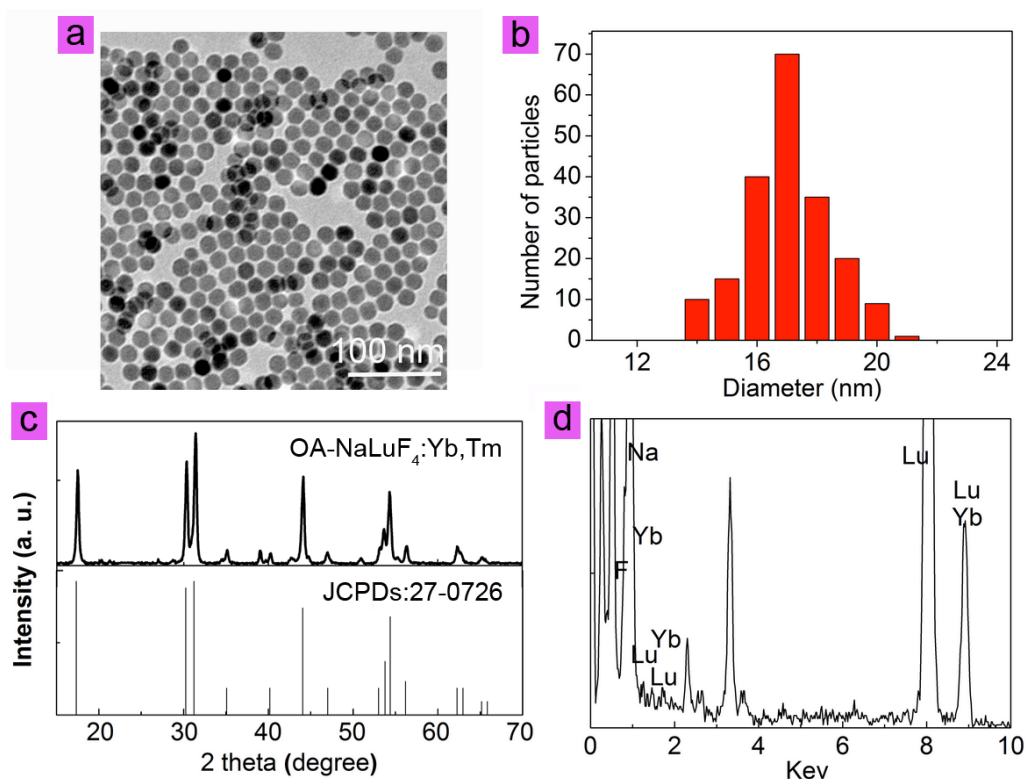


**Figure 1.** (a) TEM image, (b) particle size distribution, (c) XRD patterns, (d) EDXA of OA-NaLuF<sub>4</sub>:Yb,Tm nanoparticles.

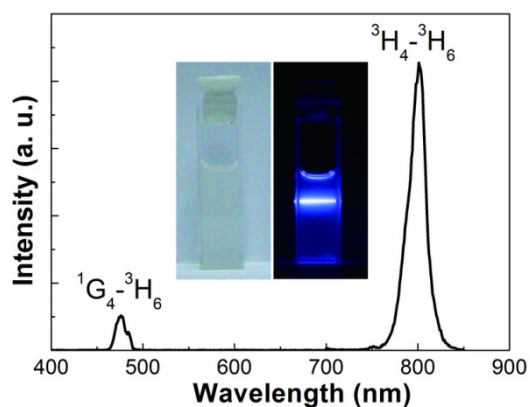


**Figure 2.** The UCL emission spectrum and photo (inset) of the OA-NaLuF<sub>4</sub>:Yb,Tm in cyclohexane solution under excitation at CW 980 nm.

The cit-NaLuF<sub>4</sub>:Yb,Tm was then applied in lymphatic vessel imaging by UCL imaging and X-ray CT imaging. Generally, ambient light should be blocked by performing the imaging experiments in a dark box to increase the SNR. The commercial lamp is commonly based on three band fluorescence, which generates the luminescence spectrum (pink) as shown in Fig. 3b. Because the emission at 800 nm is weak from ambient light, UCL imaging employed 800 nm

emission as signal will show better SNR than in the visible light range (Fig. 3b, purple). To investigate whether or not the lymph vessel can be imaged in ambient light, the location of the lymph vessel was firstly determined using UCL imaging. Fifty microliters of cit-NaLuF<sub>4</sub>:Yb,Tm (2 mg/mL) was injected intradermally into the right hind limb of the mouse. Thirty minutes after the injection, the image of the lymph vessel was recorded on the *in vivo* UCL imaging system, without cutting ambient light; the image obtained was shown in Fig. 4a simply by collecting the UCL emission at 800 nm with an EMCCD, upon irradiation with a CW 980 nm laser (50 mW/cm<sup>2</sup>, Fig. 3a). An intense UCL signal could be detected at 800 nm from the lymphatic vessel (Fig. 4a) with an exposure time of 0.1 s and gain setting of 0 (Supplementary Material: Fig. S3 and video 1), clearly depicting the lymphatic drainage by UCL imaging agents cit-NaLuF<sub>4</sub>:Yb,Tm. This means the injected solution is rapidly taken into the lymphatic drainage within a few minutes and begin to reveal the lymphatic vessels around the injection sites. Three sections with identical area were selected for analysis of UCL intensity, 800 nm light from the ambient light and CCD noise by Kodak *in vivo* system software. Here the ambient light and CCD background signal are denoted as noise. The

Area 1 signal includes the UCL signal and noise, and the signal of Area 2 and Area 3 is from the noise. Because the black animal plate adsorbed the light, the signal of Area 3 is weaker than that of Area 2. Quantitative analysis showed that the UCL SNR from the lymph vessel is 3.66 (Fig. 4b). This is the first time that the photoluminescent imaging of a whole-body animal has been achieved without cutting out ambient light (Fig. 4a, video 1 and Supplementary Material: Fig. S3-S4). Moreover, this means the UCL signal could be detected with a frame per second of more than 10, which will help clinician achieve more real time dynamic imaging information.

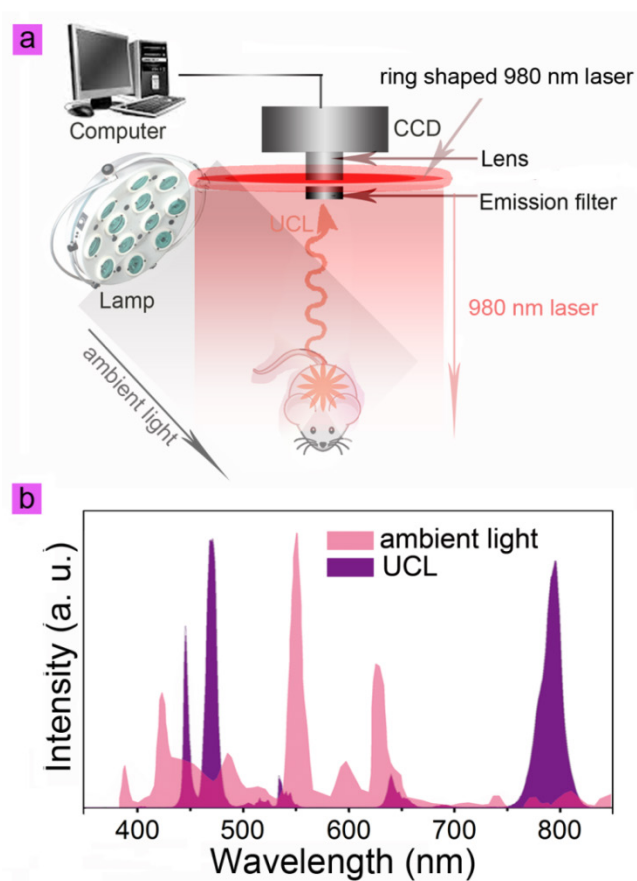


**Figure 3.** (a) The scheme depicts *in vivo* UCL imaging under lamp light. Eight external 0-5 W adjustable CW 980 nm lasers were used as the ring shaped excitation sources, and a lamp as lighting system. An Andor DU897 EMCCD with an 800 nm bandpass filter was used as the signal collector. The UCL imaging of a whole-body animal could be achieved without cutting out ambient light due to the excellent UCL emission at 800 nm of NaLuF<sub>4</sub>:Yb,Tm. (b) The luminescence spectrum of a normal lamp and UCL spectrum of NaLuF<sub>4</sub>:Yb,Tm nanoparticles.

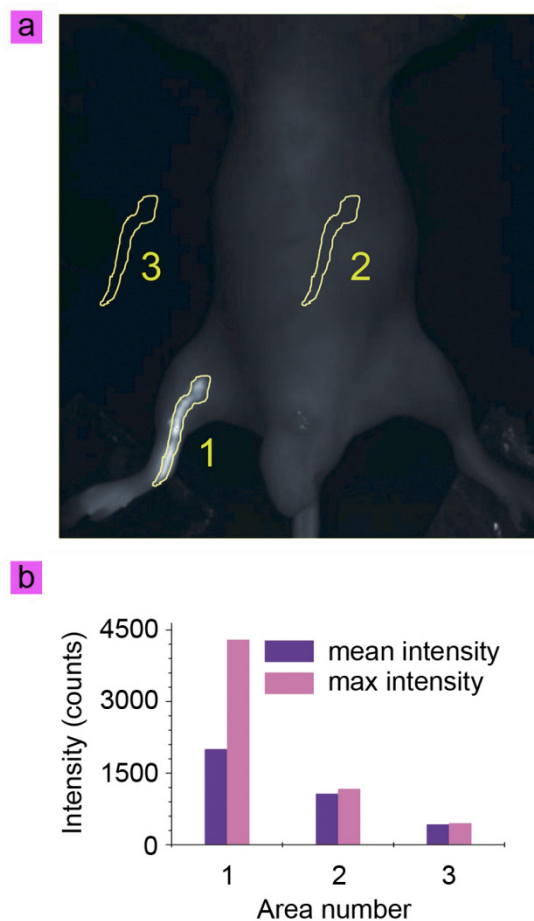


**Figure 4.** (a) *In vivo* UCL imaging of the lymphatic vessel of the cit-NaLuF<sub>4</sub>:Yb,Tm-injected mouse upon irradiation at 980 nm laser in the presence of ambient lamp. (b) Quantitative analysis of UCL intensity in the identified area shown in (a).

Although UCL imaging presents excellent imaging quality, the *in vivo* imaging resolution and 3D information is limited. And thus we try to use CT imaging to achieve more information due to the theoretical high X-ray attenuation coefficient of cit-NaLuF<sub>4</sub>:Yb,Tm.

Now there is commercial X-ray CT imaging agent to view lymphatic circulation and lymph nodes for diagnostic purposes, while the specialists observed that the pulmonary complications following lymphangiography are more often severe in patients with lymphatic obstruction. So decreasing the dosage of injection is of great significance to the lymphangiographer. To assess the X-ray imaging effects of cit-NaLuF<sub>4</sub>:Yb,Tm, we firstly quantitatively detect its X-ray absorption. Different concentration of cit-NaLuF<sub>4</sub>:Yb,Tm and the control commercial X-ray imaging agents, iopromide injection solution, was monitored by a X-ray CT to determine the specification curve of HU value. Result showed that a

cit-NaLuF<sub>4</sub>:Yb,Tm preparation of concentration 1 mg/mL is equivalent in X-ray absorption to a 1.55 mg/mL iopromide injection solution (Fig. 5), indicating the excellent X-ray CT imaging ability and potential as CT imaging agents in clinical to decrease drug dose used.

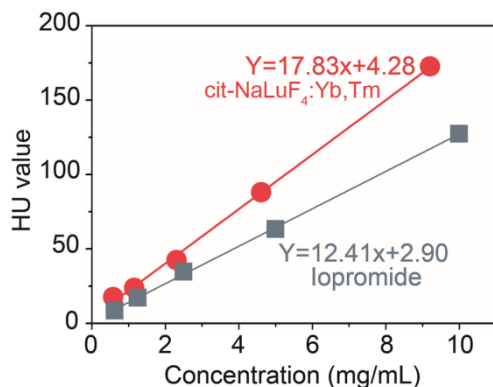


**Figure 5.** HU value to various concentration of iopromide (gray) and cit-NaLuF<sub>4</sub>:Yb,Tm (red) at room temperature detected by a Siemens CT.

CT lymphography allows accurate localization even with lymph flow rerouting toward the subsequent distant nodes and in those with multiple sentinel lymph node (SLN). To further investigate the *in vivo* X-ray CT imaging ability, the same mouse used in UCL imaging was then transferred to a Skyscan CT, and imaged for 20 min. The results shown in Fig. 6a, b, c and video 2 depicts the precise anatomical structure of the lymph vessel (Fig. 4a), without the need for dissection. The different angle views of the 3D CT image sets facilitates comprehensive perception of the anatomy of the lymphatic pathway. And the routes of CT imaged draining lymphatic vessels appears consistent with those observed on the UCL lymphatic imaging. In addition, our cit-NaLuF<sub>4</sub>:Yb,Tm are ex-

pected to have small diffusion coefficients due to the relatively large size. The slower lymphatic flow maximizes the retention time of our cit-NaLuF<sub>4</sub>:Yb,Tm in lymphatic vessels compared to small molecular CT imaging contrast such as commercial iopamidol, by which the lymphatic enhancement appears to slightly decrease on the first or second postcontrast images.[50] Furthermore, the high resolution X-ray CT imaging reveals more information by observation from different sides (Fig. 6c).

To date, although gamma probes- and vital dye-guided lymphatic mapping have shown favorable results, there are some disadvantages and potential pitfalls in lymph node or vessel biopsy with these methods. Lymphoscintigraphy shows poor spatial resolution and the lack of accurate anatomic landmarks and geometry. Gamma probe-directed lymphatic mapping may be difficult when the lymph node or vessel is close to the injection site because of shine-through radioactivity. And the blue dye-stained lymphatic vessels and/or nodes may not be readily apparent in the fatty axilla. As seen from the result above, our dual-modal imaging UCNPs presents excellent luminescence imaging depth without needs of skin removal and high SNR of luminescence without needs of cutting off ambient light. This gives more convenience of surgery operation for clinician. In addition, as supplements, the UCNPs as CT imaging agents show comprehensive perception of the anatomy of the lymphatic pathway by X-ray CT imaging in spite of a paratibial one. Furthermore, the use of nanoparticles based imaging agents has advantages such as size tunability and the surface of particles can be functionalized for improved selectivity, which may decrease toxicity due to less uptake by non-target tissues and organs.[33, 51]

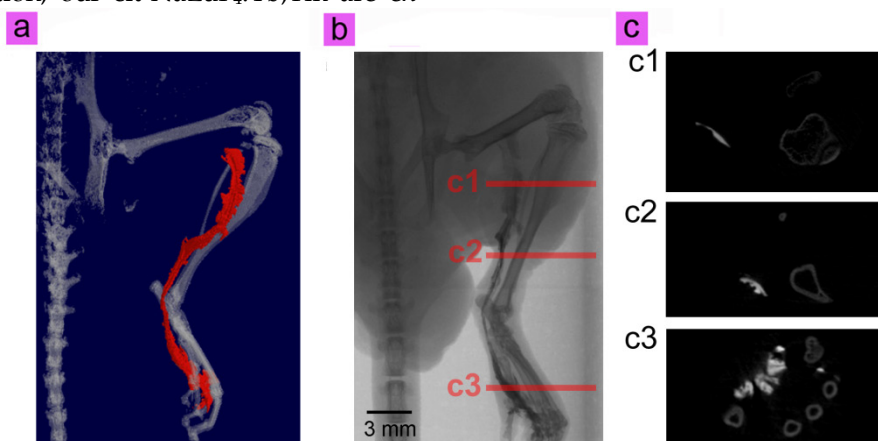


**Figure 6.** 3D reconstruction (a) and raw data (b) of *in vivo* CT imaging of the lymphatic vessel of mouse injected with cit-NaLuF<sub>4</sub>:Yb,Tm. Red line in 6a is the simulated lymphatic vessel in 6b. (c) Some special cross sections shown in 6b.

Finally, the biocompatibility of cit-NaLuF<sub>4</sub>:Yb,Tm was investigated. Varying concentrations (100-1000 µg/mL) of cit-NaLuF<sub>4</sub>:Yb,Tm was incubated with the human nasopharyngeal epidermal carcinoma cell line KB cells for 48 hours and then tested by methyl thiazolyl tetrazolium (MTT) assay. Result shown in Fig. 7 compares the effects of varying concentrations (100-1000 µg/mL) of cit-NaLuF<sub>4</sub>:Yb,Tm on KB cells and no significant difference in the proliferation of the cells were observed in the absence or presence of 0-600 µg/mL cit-NaLuF<sub>4</sub>:Yb,Tm. After 48 h of incubation with 1000 µg/mL of cit-NaLuF<sub>4</sub>:Yb,Tm, the cellular viability was greater than 90%. The MTT assay results demonstrated that the obtained cit-NaLuF<sub>4</sub>:Yb,Tm has low cytotoxicity.

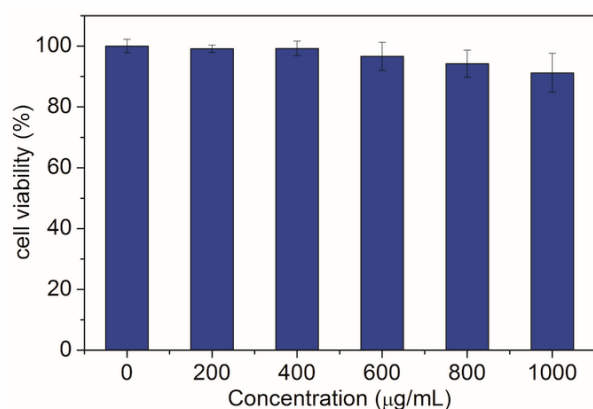


**Figure 7.** *In vitro* toxicity assessment of cit-NaLuF<sub>4</sub>:Yb,Tm by MTT assay.

In summary, we demonstrated a dual-modal imaging agent based on Yb<sup>3+</sup> and Tm<sup>3+</sup> codoped NaLuF<sub>4</sub> nanocrystals, showing bright upconversion luminescence under ambient light and high X-ray attenuation, by which the optical imaging of lymphatic vessel in ambient light is realized and its comprehensive perception of the anatomy of the lymphatic pathway is recorded. Thus, this technique appears to have an excellent potential in preoperative lymphatic mapping and imaging guided surgery.

## Supplementary Material

Fig.S1 – S4. <http://www.thno.org/v03p0346s1.pdf>

## Acknowledgements

The authors greatly acknowledge the financial support from NSFC (21231004), State Key Basic Research Program of China (2011AA03A407 and

2012CB932403), and Shanghai Sci. Tech. Comm. (11XD1400200 and 12JC1401300), IRT0911, SLADP (B108) for financial support.

## Competing Interests

The authors have declared that no competing interest exists.

## References

- Chen IY, Wu JC. Cardiovascular molecular imaging. *Circulation*. 2011; 123: 425-43.
- He M, Huang P, Zhang CL, Hu HY, Bao CC, Gao G, et al. Dual phase-controlled synthesis of uniform lanthanide-doped NaGdF<sub>4</sub> upconversion nanocrystals via an OA/ionic liquid two-phase system for *in vivo* dual-modality imaging. *Adv Funct Mater*. 2011; 21: 4470-7.
- Pan D, Schirra CO, Senpan A, Schmieder AH, Stacy AJ, Roessl E, et al. An early investigation of ytterbium nanocolloids for selective and quantitative "multicolor" spectral CT imaging. *ACS Nano*. 2012; 6: 3364-70.
- Zhou J, Zhu X, Chen M, Sun Y, Li F. Water-stable NaLuF<sub>4</sub>-based upconversion nanophosphors with long-term validity for multimodal lymphatic imaging. *Biomaterials*. 2012; 33: 6201-10.
- Yang Y, Zhao Q, Feng W, Li F. Luminescent chemodosimeters for bioimaging. *Chem. Rev*. 2012; 113: 192-270.
- Weissleder R, Pittet MJ. Imaging in the era of molecular oncology. *Nature*. 2008; 452: 580-9.
- Wang F, Banerjee D, Liu YS, Chen XY, Liu XG. Upconversion nanoparticles in biological labeling, imaging, and therapy. *Analyst*. 2010; 135: 1839-54.
- Zhou J, Liu Z, Li FY. Upconversion nanophosphors for small-animal imaging. *Chem Soc Rev*. 2012; 41: 1323-49.
- Zhu X, Zhou J, Chen M, Shi M, Feng W, Li F. Core-shell Fe<sub>3</sub>O<sub>4</sub>@NaLuF<sub>4</sub>:Yb,Er/Tm nanostructure for MRI, CT and upconversion luminescence tri-modality imaging. *Biomaterials*. 2012; 33: 4618-27.
- Chatterjee DK, Rufalhah AJ, Zhang Y. Upconversion fluorescence imaging of cells and small animals using lanthanide doped nanocrystals. *Biomaterials*. 2008; 29: 937-43.
- Yang Y, Sun Y, Cao T, Peng J, Liu Y, Wu Y, et al. Hydrothermal synthesis of NaLuF<sub>4</sub>:<sup>152</sup>Sm,Yb,Tm nanoparticles and their application in dual-modality upconversion luminescence and SPECT bioimaging. *Biomaterials*. 2013; 34: 774-83.
- Sun Y, Yu MX, Liang S, Zhang YJ, Li CG, Mou TT, et al. Fluorine-18 labeled rare-earth nanoparticles for positron emission tomography (PET) imaging of sentinel lymph node. *Biomaterials*. 2011; 32: 2999-3007.
- Zhou J, Sun Y, Du XX, Xiong LQ, Hu H, Li FY. Dual-modality *in vivo* imaging using rare-earth nanocrystals with near-infrared to near-infrared (NIR-to-NIR) upconversion luminescence and magnetic resonance properties. *Biomaterials*. 2010; 31: 3287-95.
- Liu Y, Ai K, Liu J, Yuan Q, He Y, Lu L. A high-performance ytterbium-based nanoparticulate contrast agent for *in vivo* X-ray computed tomography imaging. *Angew Chem Int Ed*. 2012; 51: 1437-42.
- Chen F, Bu WB, Zhang SJ, Liu XH, Liu JN, Xing HY, et al. Positive and negative lattice shielding effects co-existing in Gd (III) ion doped bifunctional upconversion nanoproboscopes. *Adv Funct Mater*. 2011; 21: 4285-94.
- Ju Q, Tu D, Liu Y, Li R, Zhu H, Chen J, et al. Amine-functionalized lanthanide-doped KGdF<sub>4</sub> nanocrystals as potential optical/magnetic multimodal bioprobes. *J Am Chem Soc*. 2011; 134: 1323-30.
- Auzel F. Upconversion and anti-stokes processes with f and d ions in solids. *Chem. Rev*. 2004; 104: 139-73.
- Haase M, Schäfer H. Upconverting nanoparticles. *Angew Chem, Int Ed*. 2011; 50: 5808-29.
- Li CX, Lin J. Rare earth fluoride nano-/microcrystals: synthesis, surface modification and application. *J Mater Chem*. 2010; 20: 6831-47.
- Mader HS, Kele P, Saleh SM, Wolfbeis OS. Upconverting luminescent nanoparticles for use in bioconjugation and bioimaging. *Curr Opin Chem Biol*. 2010; 14: 582-96.
- Wang GF, Peng Q, Li YD. Lanthanide-doped nanocrystals: Synthesis, optical-magnetic properties, and applications. *Acc Chem Res*. 2011; 44: 322-32.
- Zhang C, Zhou HP, Liao LY, Feng W, Sun W, Li ZX, et al. Luminescence modulation of ordered upconversion nanopatterns by a photochromic

- diarylethene: rewritable optical storage with nondestructive readout. *Adv Mater.* 2010; 22: 633-7.
23. Xia A, Gao Y, Zhou J, Li CY, Yang TS, Wu DM, et al. Core-shell NaYF<sub>4</sub>:Yb<sup>3+</sup>,Tm<sup>3+</sup>@FexOynanocrystals for dual-modality T<sub>2</sub>-enhanced magnetic resonance and NIR-to-NIR upconversion luminescent imaging of small-animal lymphatic node. *Biomaterials.* 2011; 32: 7200-8.
  24. Peng J, Sun Y, Liu Q, Yang Y, Zhou J, Feng W, et al. Upconversion nanoparticles dramatically promote plant growth without toxicity. *Nano Res.* 2012; 5: 770-82.
  25. Liu Y, Zhou S, Tu D, Chen Z, Huang M, Zhu H, et al. Amine-functionalized lanthanide-doped zirconia nanoparticles: optical spectroscopy, time-resolved fluorescence resonance energy transfer biodetection, and targeted imaging. *J Am Chem Soc.* 2012; 134: 15083-90.
  26. Liu Q, Sun Y, Yang TS, Feng W, Li CG, Li FY. Sub-10 nm hexagonal lanthanide-doped NaLuF<sub>4</sub> upconversion nanocrystals for sensitive bioimaging *in vivo*. *J Am Chem Soc.* 2011; 133: 17122-5.
  27. Wang F, Liu XG. Upconversion multicolor fine-tuning: Visible to near-infrared emission from lanthanide-doped NaYF<sub>4</sub> nanoparticles. *J Am Chem Soc.* 2008; 130: 5642-3.
  28. Park YI, Kim JH, Lee KT, Jeon KS, Bin Na H, Yu JH, et al. Nonblinking and nonbleaching upconverting nanoparticles as an optical imaging nanoprobe and T1 magnetic resonance imaging contrast agent. *Adv Mater.* 2009; 21: 4467-71.
  29. Wu SW, Han G, Milliron DJ, Aloni S, Altoe V, Talapin DV, et al. Non-blinking and photostable upconverted luminescence from single lanthanide-doped nanocrystals. *P Natl Acad Sci USA.* 2009; 106: 10917-21.
  30. Yu MX, Li FY, Chen ZG, Hu H, Zhan C, Yang H, et al. Laser scanning up-conversion luminescence microscopy for imaging cells labeled with rare-earth nanophosphors. *Anal Chem.* 2009; 81: 930-5.
  31. Liu R, Tu D, Liu Y, Zhu H, Li R, Zheng W, et al. Controlled synthesis and optical spectroscopy of lanthanide-doped KLaF<sub>4</sub> nanocrystals. *Nanoscale.* 2012; 4: 4485-91.
  32. Nyk M, Kumar R, Ohulchanskyy TY, Bergey EJ, Prasad PN. High contrast *in vitro* and *in vivo* photoluminescence bioimaging using near infrared to near infrared up-conversion in Tm<sup>3+</sup> and Yb<sup>3+</sup> doped fluoride nanophosphors. *Nano Lett.* 2008; 8: 3834-8.
  33. Xiong LQ, Chen ZG, Tian QW, Cao TY, Xu CJ, Li FY. High contrast upconversion luminescence targeted imaging *in vivo* using peptide-labeled nanophosphors. *Anal Chem.* 2009; 81: 8687-94.
  34. Lim SF, Riehn R, Ryu WS, Khanarian N, Tung CK, Tank D, et al. In vivo and scanning electron microscopy imaging of upconverting nanophosphors in *Caenorhabditis elegans*. *Nano Lett.* 2006; 6: 169-74.
  35. Yang T, Sun Y, Liu Q, Feng W, Yang P, Li F. Cubic sub-20 nm NaLuF<sub>4</sub>-based upconversion nanophosphors for high-contrast bioimaging in different animal species. *Biomaterials.* 2012; 33: 3733-42.
  36. Gorris HH, Ali R, Saleh SM, Wolfbeis OS. Tuning the dual emission of photon-upconverting nanoparticles for ratiometric multiplexed encoding. *Adv Mater.* 2011; 23: 1652-5.
  37. Liu YS, Tu DT, Zhu HM, Li RF, Luo WQ, Chen XY. A strategy to achieve efficient dual-mode luminescence of Eu<sup>3+</sup> in lanthanides doped multifunctional NaGdF<sub>4</sub> nanocrystals. *Adv Mater.* 2010; 22: 3266-71.
  38. Mahalingam V, Vetrone F, Naccache R, Speghini A, Capobianco JA. Colloidal Tm<sup>3+</sup>/Yb<sup>3+</sup>-doped LiYF<sub>4</sub> nanocrystals: Multiple luminescence spanning the UV to NIR regions via low-energy excitation. *Adv Mater.* 2009; 21: 4025-8.
  39. Schafer H, Ptacek P, Eickmeier H, Haase M. Synthesis of hexagonal Yb<sup>3+</sup>,Er<sup>3+</sup>-doped NaYF<sub>4</sub> nanocrystals at low temperature. *Adv Funct Mater.* 2009; 19: 3091-7.
  40. Wang F, Han Y, Lim CS, Lu YH, Wang J, Xu J, et al. Simultaneous phase and size control of upconversion nanocrystals through lanthanide doping. *Nature.* 2010; 463: 1061-5.
  41. Jin JF, Gu YJ, Man CWY, Cheng JP, Xu ZH, Zhang Y, et al. Polymer-coated NaYF<sub>4</sub>: Yb<sup>3+</sup>, Er<sup>3+</sup> upconversion nanoparticles for charge-dependent cellular imaging. *ACS Nano.* 2011; 5: 7838-47.
  42. Cheng L, Yang K, Li YG, Chen JH, Wang C, Shao MW, et al. Facile preparation of multifunctional upconversion nanoprobe for multimodal imaging and dual-targeted photothermal therapy. *Angew Chem, Int Ed.* 2011; 50: 7385-90.
  43. Chen G, Shen J, Ohulchanskyy TY, Patel NJ, Kutikov A, Li Z, et al. (α-NaYbF<sub>4</sub>:Tm<sup>3+</sup>)/CaF<sub>2</sub> core/shell nanoparticles with efficient near-infrared to near-infrared upconversion for high-contrast deep tissue bioimaging. *ACS Nano.* 2012; 6: 8280-7.
  44. Yang YM, Shao Q, Deng RR, Wang C, Teng X, Cheng K, et al. *In vitro* and *in vivo* uncaging and bioluminescence imaging by using photocaged upconversion nanoparticles. *Angew Chem Int Ed.* 2012; 51: 3125-9.
  45. Mueller-Lisse UG, Scher B, Scherr MK, Seitz M. Functional imaging in penile cancer: PET/computed tomography, MRI, and sentinel lymph node biopsy. *Curr Opin Urol.* 2008; 18: 105-10.
  46. Niu G, Zhang F, Lu GM, Chen XY. Preclinical lymphatic imaging. *Mol Imaging Biol.* 2011; 13: 599-612.
  47. Brooks RA, Chiro GD. Principles of computer assisted tomography (CAT) in radiographic and radioisotopic imaging. *Phys Med Biol.* 1976; 21: 689.
  48. Bogdan N, Vetrone F, Ozin GA, Capobianco JA. Synthesis of ligand-free colloidal stable water dispersible brightly luminescent lanthanide-doped upconverting nanoparticles. *Nano Lett.* 2011; 11: 835-40.
  49. Cao TY, Yang TS, Gao Y, Yang Y, Hu H, Li FY. Water-soluble NaYF<sub>4</sub>:Yb/Er upconversion nanophosphors: synthesis, characteristics and application in bioimaging. *Inorg Chem Commun.* 2010; 13: 392-4.
  50. Suga K, Yuan Y, Okada M, Matsunaga N, Tangoku A, Yamamoto S, et al. Breast sentinel lymph node mapping at CT lymphography with iopamidol: Preliminary experience. *Radiology.* 2004; 230: 543-52.
  51. Zeng JH, Su J, Li ZH, Yan RX, Li YD. Synthesis and upconversion luminescence of hexagonal-phase NaYF<sub>4</sub>: Yb<sup>3+</sup>, Er<sup>3+</sup>, phosphors of controlled size and morphology. *Adv Mater.* 2005; 17: 2119-23.